Retrieval of Aerosol Optical Properties from Multi-Angle Satellite Imagery

John V. Martonchik and David J. Diner

Abstract—**Optical properties of tropospheric aerosols, such as their opacity, single-scattering albedo, and phase function are needed for studies of their effects on the solar radiation budget at the Earth's surface and as input to surface reflectance retrieval algorithms designed to correct top-of-atmosphere imagery for atmospheric effects. Using simulation multi-angle imagery, we have been investigating a new method for retrieving atmospheric aerosol optical properties over land. The described method makes use of the presence of spatial contrasts within the imagery, and compares the spatial Fourier transforms of the multi-angle images at zero and nonzero spatial frequencies. An initial guess for the aerosol properties is made and the Fourier components of the surface reflectance distribution are retrieved at zero and nonzero frequencies. A comparison of the angular shape of the retrieved functions is then used to establish whether the initial guess for the aerosol parameters was correct. Other than the need to define a relationship between the angular variation of the Fourier transform of the intrinsic surface angular reflectance at the zero and nonzero frequencies, the method assumes no *a priori* knowledge about the aerosols or surface characteristics. We discuss sensitivities to various aerosol properties.**

I. Introduction

THE global nature of the problems facing our planet and the many feedback mechanisms governing the interaction between the land surface, atmosphere, and oceans indicate a clear role for remote sensing. The Earth Observing System (EOS) represents one facet of an international research program into the causes and effects of global change. One of the instruments selected for the first polar platform, EOS-A1, is the Multi-angle Imaging SpectroRadiometer, MISR [1]. MISR will provide routine, systematic, and global multi-angle imaging of the Earth in four spectral bands (440, 550, 670, and 860 nm), using an array of cameras pointed toward the nadir and forward and aftward along the spacecraft ground track. Within a 7-min period, every point in a 350-km swath will be imaged at all viewing angles, ensuring observations acquired under virtually identical illumination and atmospheric conditions. Global multi-angle imagery will be obtained with a pixel sample spacing of 1.92 km, and selected regions will be observed with 240-m sampling. Global coverage will be acquired in 9 days. Among other applications, MISR will provide a systematic means of characterizing radiative properties of the land surface and the atmosphere and separating their respective contributions to remote sensing imagery.

Quantitative studies of the surface from space using MISR will require the ability to infer surface directional reflectance distributions and hemispherical albedos. Such measurements are needed for climate modeling and studies of biosphere–atmosphere interactions [2], [3]. Unfortunately, it is not possible to observe these surface quantities directly from a platform situated above the top of the atmosphere (TOA). Scattering and absorption by aerosols are responsible for substantial modifications of the absolute radiances and spectral content of remotely sensed images of the Earth's surface. Attenuation of sunlight resulting from scattering and absorption losses within the incident and reflected beams is offset by scattered radiance resulting from light which has been (1) reflected by the atmosphere without reaching the surface (path radiance), (2) subjected to multiple reflections between the atmosphere and surface, and (3) scattered into the line of sight from the neighboring terrain. Thus, reductions of data from MISR and other EOS surface imaging instruments to absolute values of the surface reflectance, suitable for long time series analysis of changes in the Earth's surface properties, will require understanding and compensation for atmospheric effects. In contrast to the open ocean, where the effects of the atmosphere on spaceborne imagery can be accounted for without requiring determination of the absolute optical properties of the marine aerosols [4], the reflectance heterogeneity, anisotropy, and variability in land surface covers preclude extension of such algorithms to the solid Earth. Thus, retrieval of spectral and directional reflectances and hemispherical albedo over land scenes will require determination of the bulk optical properties of the continental aerosols, including the optical depth τ, single-scattering albedo, w, and a parametric representation of either the size distribution or the scattering phase function. This information must then be used in an inversion scheme based on radiative transfer theory to derive the surface properties. In this paper, we describe the results of an investigation into a novel technique for performing such retrievals. Multi-angle imagery, such as that to be obtained by MISR, is assumed. This enables consideration of algorithms which would be unavailable to solely nadir-viewing instruments.

II. Theoretical Background

For a radiometrically calibrated satellite image, the measured radiance I can be written as

$$I(x, y; \mu, \mu_0, \phi-\phi_0) = R(\mu, \mu_0, \phi-\phi_0)$$

Manuscript received June 1, 1991; revised September 26, 1991.

This work was carried out by the Jet Propulsion Laboratory, California Institute of Technology, under contract with the National Aeronautics and Space Administration.

J. V. Martonchik and D. J. Diner are with the Jet Propulsion Laboratory, California Institute of Technology, Pasadena, CA 91109.

IEEE Log Number 9105696.

$$+ \exp(-\tau/\mu)\cdot\pi^{-1}\int_0^1\int_0^{2\pi} r(x,y;\mu,\mu',\phi-\phi') \cdot D(\mu',\mu_0,\phi'-\phi_0)\mu'\,d\mu'\,d\phi' + \pi^{-1}\int_0^1\int_0^{2\pi}\int_0^1\int_0^{2\pi} T(x,y;\mu,\mu'',\phi-\phi'') \otimes r(x,y;\mu'',\mu',\phi''-\phi')D(\mu',\mu_0,\phi'-\phi_0) \cdot \mu'\,d\mu''\,d\phi''\,d\mu''\,d\phi'' \quad (1)$$

where x, y are the image spatial coordinates, μ and μ_0 are the cosines of the view and Sun angles, and $\phi-\phi_0$ is the view azimuthal angle with respect to the Sun position. The properties of the atmosphere are assumed to be horizontally homogeneous. On the right-hand side of (1), R is the radiance field scattered by the atmosphere to space without interacting with the surface, τ is the opacity of the atmosphere, D is the direct and downward diffuse radiance field incident on the surface, T is the upward diffuse transmittance, and r is the spatially variable surface directional reflectance. Although multiple reflections between the surface and atmosphere will cause some spatial variability in D, this can be ignored for practical purposes. the transmittance T is written as spatially varying and with the convolution operation $\otimes$ describes the blurring effect of the atmosphere on the surface reflectance r [5]. Since the blurring scale length is of the order of the effective scale height of the scattering opacity of the atmosphere, images of a surface overlain by an atmosphere with an opacity dominated by tropospheric aerosols (scale height $\sim$1–2 km) will have a nonnegligible blurred component if the image spatial resolution is less than $\sim$1 km. This is the 3-D radiative transfer regime [6]–[8]. On the other hand, when the image spatial resolution is greater than $\sim$2 km no significant blurring is expected and the transmittance T is effectively a delta function in the spatial coordinates. This is the standard 1-D radiative transfer regime.

Because of the convolution operation in (1), it is more convenient to work in the spatial Fourier transform domain. Applying a spatial Fourier transform to (1), we obtain

$$\boldsymbol{I}(u,v;\mu,\mu_0,\phi-\phi_0) = R(\mu,\mu_0,\phi-\phi_0)\delta_{0u}\delta_{0v} + \exp(-\tau/\mu)\cdot\pi^{-1}\int_0^1\int_0^{2\pi}\mathbf{r}(u,v;\mu,\mu',\phi-\phi') \cdot D(\mu',\mu_0,\phi'-\phi_0)\mu'\,d\mu'\,d\phi' + \pi^{-1}\int_0^1\int_0^{2\pi}\int_0^1\int_0^{2\pi}\mathbf{T}(u,v;\mu,\mu'',\phi-\phi'') \cdot \mathbf{r}(u,v;\mu'',\mu',\phi''-\phi') \cdot D(\mu',\mu_0,\phi'-\phi_0)\mu'\,d\mu''\,d\phi''\,d\mu'\,d\phi' \quad (2a)$$

where u, v are the spatial frequency wavenumbers corresponding to the x and y coordinates, the boldface symbols represent transformed variables, and δ is the Kronecker delta. In the 3-D radiative transfer regime $\mathbf{T}$ drops off in magnitude with increasing wavenumber, thus acting like a low-pass filter for the surface reflectance spatial structure [5]. For those wavenumbers outside the bandpass, (2a) then can be written as

$$\mathbf{I}(u,v;\mu,\mu_0,\phi-\phi_0) = \exp(-\tau/\mu)\cdot\pi^{-1}\int_0^1\int_0^{2\pi}\mathbf{r}(u,v;\mu,\mu',\phi-\phi_0) \cdot D(\mu',\mu_0,\phi'-\phi_0)\mu'\,d\mu'\,d\phi'. \quad (2b)$$

In the 1-D radiative transfer regime $\mathbf{T}$ is independent of wavenumber and the top-of-atmosphere radiance is given by

$$\mathbf{I}(u,v;\mu,\mu_0,\phi-\phi_0) = R(\mu,\mu_0,\phi-\phi_0)\delta_{0u}\delta_{0v} + \exp(-\tau/\mu)\cdot\pi^{-1}\int_0^1\int_0^{2\pi}\mathbf{r}(u,v;\mu,\mu',\phi-\phi') \cdot D(\mu',\mu_0,\phi'-\phi_0)\mu'\,d\mu'\,d\phi' + \pi^{-1}\int_0^1\int_0^{2\pi}\int_0^1\int_0^{2\pi}T(\mu,\mu'',\phi-\phi'')\mathbf{r}(u,v;\mu'',\mu',\phi''-\phi') \cdot D(\mu',\mu_0,\phi'-\phi_0)\mu'\,d\mu''\,d\phi''\,d\mu'\,d\phi' \quad (2c)$$

where the 1–D transmittance

$$T(\mu,\mu'',\phi-\phi'') = \mathbf{T}(0,0;\mu,\mu'',\phi-\phi'').$$

III. Simplied Aerosol Retrieval Algorithm

The above equations represent the situation in which the surface reflectance distribution contains spatial contrasts, such that there is nonzero spatial frequency information in the images. The atmospheric retrieval algorithm described in this paper takes advantage of the different information contained in the zero and nonzero spatial frequency radiation fields. For example, the path radiance term R exists in these equations only for zero wavenumber. The algorithm also takes advantage of the assumption that multi-angle imagery is acquired, and uses this additional dimension to constrain the retrievals. In brief, the algorithm starts with an initial guess for the aerosol optical properties (opacity, single-scattering albedo, and phase function). The Fourier components of the surface directional reflectance are then retrieved for both zero and nonzero spatial frequencies. The criterion used to establish whether the initial guess for the aerosol parameters was correct is a comparison of the angular shape of the retrieved functions. If the shapes for zero and nonzero frequencies do not satisfy a specified relationship, it is assumed that this is due to an incorrect guess for the atmospheric parameters. These parameters are updated and the process is repeated until the relationship between the shapes of the retrieved directional reflectance functions is satisfied. In this section, the algorithm is described in detail, using the theoretical background presented above.

Given a set of images I taken at various view geometries (different μ and $\phi-\phi_0$), it is straightforward to invert (2a), (2b), or (2c) for the transformed directional reflectance $\mathbf{r}$ if the atmospheric scattering properties are specified. To carry out the inversion, it is convenient to express the azimuthal dependence of the surface directional reflectance in some analytic form to facilitate the integration procedures in the equations. We have

chosen the simple expression

$$r(x,y;\mu,\mu',\phi-\phi') = r^0(x,y;\mu) + r^1(x,y;\mu)\cos(\phi-\phi') \tag{3a}$$

$$\mathbf{r}(u,v;\mu,\mu',\phi-\phi') = \mathbf{r}^0(u,v;\mu) + \mathbf{r}^1(u,v;\mu)\cos(\phi-\phi') \tag{3b}$$

where both r^0 and r^1 (or $\mathbf{r}^0$ and $\mathbf{r}^1$) can be determined when the viewing geometry is not limited to only one azimuth angle. Note that the assumed functional form is independent of incident angle μ'. This is appropriate for observations acquired at a fixed Sun angle since the surface directional reflectance in (1) and (2a–c) is multiplied by the direct and diffuse downward radiance field D and then integrated over angle, which means that the dependence on μ' cannot be directly ascertained by the retrieval process.

The case in which the surface reflectance distribution is characterized by a variation in albedo from pixel to pixel but with a single non-Lambertian normalized directional reflectance function for the entire scene was investigated by Martonchik *et al.* [9]. Although this constitutes a somewhat idealized representation of what occurs in nature, examination of this case is a good starting point to test the validity of the algorithm. We shall review the results of Martonchik *et al.* [9], and then examine the more realistic situation in which not only the albedo, but also the shape of the directional reflectance function, is allowed to vary from one pixel to another. For the single non-Lambertian case, the relationship between zero and nonzero wavenumber directional reflectances is clear. When

$$\mathbf{r}(x,y;\mu,\mu',\phi-\phi') = \mathbf{A}(x,y)r_n(\mu,\mu',\phi-\phi') \tag{4a}$$

$$= \mathbf{A}(x,y)\left[r_n^0(\mu) + r_n^1(\mu)\cos(\phi-\phi')\right] \tag{4b}$$

then

$$\mathbf{r}(0,0;\mu,\mu',\phi-\phi') = \mathbf{A}(0,0)r_n(\mu,\mu',\phi-\phi') \tag{4c}$$

$$\mathbf{r}(u,v;\mu,\mu',\phi-\phi') = \mathbf{A}(u,v)r_n(\mu,\mu',\phi-\phi') \tag{4d}$$

where $\mathbf{A}$ is the transformed hemispherical albedo of the surface image and $\mathbf{r}_n$ is the single, spatially invariant, normalized directional reflectance described by (3). The two expressions in (4c) and (4d) obviously have the same angular shape and it is this condition which was tested in the atmospheric retrieval algorithm described in [9]. Inserting (3) and (4) into (2a), the retrieval equations can be written as

$$\begin{aligned}\mathbf{I}(0,0;\mu,\mu_0,\phi-\phi_0) = {} & R(\mu,\mu_0,\phi-\phi_0) \\ & + \exp(-\tau/\mu)\mathbf{A}(0,0) \\ & \cdot \left[S_0 r_n^0(\mu) + S_1(\phi-\phi_0)r_n^1(\mu)\right] \\ & + \mathbf{A}(0,0)S_0 \int_0^1\int_0^{2\pi} r_n^0(\mu'')\mathbf{T} \\ & \cdot (0,0;\mu,\mu'',\phi-\phi'')\,d\mu''\,d\phi'' \\ & + \mathbf{A}(0,0)\int_0^1\int_0^{2\pi} S_1(\phi''-\phi_0)r_n^1(\mu'')\mathbf{T} \\ & \cdot (0,0;\mu,\mu'',\phi-\phi'')\,d\mu''\,d\phi'' \end{aligned} \tag{5a}$$

$$\begin{aligned}\mathbf{I}(u,v;\mu,\mu_0,\phi-\phi_0) = {} & \exp(-\tau/\mu)\mathbf{A}(u,v) \\ & \cdot \left[S_0 r_n^0(\mu) + S_1(\phi-\phi_0)r_n^1(\mu)\right] \\ & + \mathbf{A}(u,v)S_0 \int_0^1\int_0^{2\pi} r_n^0(\mu'')\mathbf{T} \\ & \cdot (u,v;\mu,\mu'',\phi-\phi'')\,d\mu''\,d\phi'' \\ & + \mathbf{A}(u,v)\int_0^1\int_0^{2\pi} S_1(\phi''-\phi_0)r_n^1(\mu'')\mathbf{T} \\ & \cdot {}_{2\pi}(u,v;\mu,\mu'',\phi-\phi'')\,d\mu''\,d\phi'' \end{aligned} \tag{5b}$$

where

$$S_0 = \pi^{-1}\int_0^1\int_0^{2\pi} D(\mu',\mu_0,\phi'-\phi_0)\mu'\,d\mu'\,d\phi' \tag{6}$$

and

$$S_1(\phi-\phi_0) = \pi^{-1}\int_0^1\int_0^{2\pi}\cos(\phi-\phi') \cdot D(\mu',\mu_0,\phi'-\phi_0)\mu'\,d\mu'\,d\phi'. \tag{7}$$

For wavenumbers u, v outside the effective bandpass of $\mathbf{T}$, (5b) can be simplified to

$$\begin{aligned}\mathbf{I}(u,v;\mu,\mu_0,\phi-\phi_0) = {} & \exp(-\tau/\mu) \\ & \cdot \mathbf{A}(u,v)\left[S_0 r_n^0(\mu) + S_1(\phi-\phi_0)r_n^1(\mu)\right].\end{aligned} \tag{5c}$$

In the analysis described in [9], (5a) and (5c) were used to retrieve $\mathbf{A}(u,v)r_n^0$ and $\mathbf{A}(u,v)r_n^1$ using simulated MISR images computed under the assumption of 3-D radiative transfer [6]–[7]. From (5c)

$$|\mathbf{A}(u,v)|r^0(\mu) = \frac{|\mathbf{I}(u,v;\mu,\mu_0,\phi_1-\phi_0)|S_1(\phi_2-\phi_0) - |\mathbf{I}(u,v;\mu,\mu_0,\phi_2-\phi_0)|S_1(\phi_1-\phi_0)}{\exp(-\tau/\mu)[S_1(\phi_2-\phi_0) - S_1(\phi_1-\phi_0)]S_0} \tag{8}$$

$$|\mathbf{A}(u,v)|r_n^1(\mu) = \frac{|\mathbf{I}(u,v;\mu,\mu_0,\phi_1-\phi_0)| - |\mathbf{I}(u,v;\mu,\mu_0,\phi_2-\phi_0)|}{\exp(-\tau/\mu)[S_1(\phi_1-\phi_0) - S_1(\phi_2-\phi_0)]} \tag{9}$$

where ϕ_1 and ϕ_2 are two distinct azimuth angles at which the observations are made. Note that complex number analysis is avoided by taking absolute values.

The retrieval of $\mathbf{A}(0,0)r_n^0(\mu)$ and $\mathbf{A}(0,0)r_n^1(\mu)$ using (5a) is also straightforward but requires an iteration scheme. We start by setting $\mathbf{A}(0,0)r_n^0$ and $\mathbf{A}(0,0)r_n^1$ equal to zero in the integral terms on the rignt-hand side of (5a) and solving for the first estimate of $\mathbf{A}(0,0)r_n^0$ and $\mathbf{A}(0,0)r_n^1$ using the remaining expression. These first estimates are then inserted into the equation to compute the integral terms, which are then subtracted from the left-hand side of (5a) and an updated $\mathbf{A}(0,0)r_n^0$ and $\mathbf{A}(0,0)r_n^1$ are calculated using the exponential term. If continued, this iteration procedure will converge

slowly, oscillating about too small and too large values for $\mathbf{A}(0,0)r_n^0(\mu)$ and $\mathbf{A}(0,0)r_n^1(\mu)$. The problem is alleviated by averaging together the previous two estimates and using that result instead of just the last estimate in the integral terms. When this is done, only three or four iterations are required for convergence. This iteration scheme can also be used when u, v are within the wavenumber bandpass defining the transmittance T, and (5b) is the appropriate retrieval equation instead of (5c). Because of $\mathbf{T}$ in the integrals of (5b), the complex $\mathbf{A}(\mathrm{u},\mathrm{v})r_n^0(\mu)$ and $\mathbf{A}(\mathrm{u},\mathrm{v})r_n^1(\mu)$ are estimated with each iteration. Upon convergence, the absolute values of the results are used.

When the images can be analyzed in the 1-D radiative transfer regime, then the appropriate equation for the retrieval of $|\mathbf{A}(u,v)|r_n^0(\mu)$ and $|\mathbf{A}(u,v)|r_n^1(\mu)$ is

$$\begin{aligned}|\mathbf{I}(u,v;\mu,\mu_0,\phi{-}\phi_0)| &= \exp(-\tau/\mu)|\mathbf{A}(u,v)| \\ &\quad\cdot\left[S_0 r_n^0(\mu) + S_1(\phi{-}\phi_0)r_n^1(\mu)\right] \\ &\quad + |\mathbf{A}(u,v)|S_0\int_0^1\int_0^{2\pi} r_n^0(\mu'')T(\mu,\mu'',\phi{-}\phi'')\,d\mu''\,d\phi'' \\ &\quad + |\mathbf{A}(u,v)|\int_0^1\int_0^{2\pi} S_1(\phi''{-}\phi_0)r_n^1(\mu'')T(\mu,\mu'',\phi{-}\phi'')\,d\mu''\,d\phi'' \end{aligned} \tag{5d}$$

where T is the 1-D transmittance. Aside from the absence of the path radiance R on the right-hand side, this expression is similar to (5a) and therefore is solved by the same iterative procedure.

The aerosol retrieval algorithm for a single normalized surface directional reflectance in the image set is summarized as follows:

Step 1

Guess an atmosphere and compute the corresponding 1-D path radiance, R, the upward directed diffuse transmittance T, and the total downward directed radiance D assuming no surface reflectance.

Step 2

Using the zero spatial frequency component of the Fourier transformed multi-angle images, iterate (5a) to solve for $\mathbf{A}(0,0)r_n^0(\mu)$ and $\mathbf{A}(0,0)r_n^1(\mu)$. The surface directional reflectance $\mathbf{r}(0,0;\mu,\phi{-}\phi')$ is then constructed according to (4) and used to update the total downward directed radiance D and to recalculate the S_0 and S_1 functions. The iteration procedure for determining $\mathbf{A}(0,0)r_n^0(\mu)$ and $\mathbf{A}(0,0)r_n^1(\mu)$ is repeated to update the atmosphere–surface functions, continuing this cycle until convergence of the function D is achieved.

Step 3

At nonzero spatial frequencies, solve for $|\mathbf{A}(u,v)|r_n^0(\mu)$ and $|\mathbf{A}(u,v)|r_n^1(\mu)$ using (8) and (9) or by iterating (5b) or (5d). The surface reflectance $|\mathbf{r}(u,v;\mu,\phi{-}\phi')|$ is then constructed according to (4) and the result compared to $\mathbf{r}(0,0;\mu,\phi{-}\phi')$ determined from Step 2. Making use of (4c) and (4d) which state that the shapes of $\mathbf{r}(0,0;\mu,\phi{-}\phi')$ and $|\mathbf{r}(u,v;\mu,\phi{-}\phi')|$ should be identical, this comparison is the basis for deciding whether the selected atmosphere in Step 1 is correct or should be updated. If the atmosphere is modified, the whole procedure from Steps 1 through 3 then is repeated until the comparison test is satisfied. The comparison test is a least squares analysis where $|\mathbf{r}(u,v;\mu,\phi{-}\phi')|$ is scaled to best match $\mathbf{r}(0,0;\mu,\phi{-}\phi')$ for the angles of the observations. This scaling is necessary because the magnitude of the albedo spectrum is not known *a priori*. The "best fit" (minimum variance) atmosphere is assumed to be the best estimate of the true atmosphere.

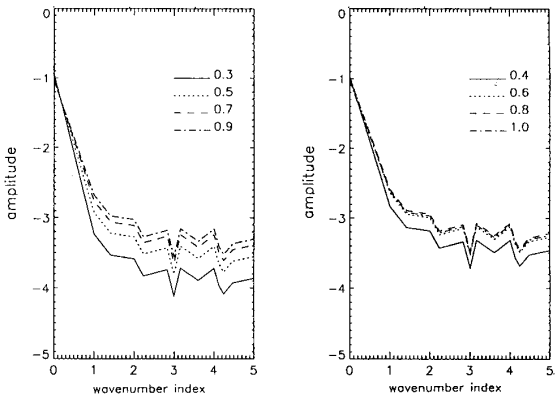

Fig. 1. Log of amplitude spectra for the simulated scene containing a single directional reflectance.

The aerosol retrieval algorithm was applied to a set of simulate multi-angle images of the Wind River Basin, WY containing only a single nonlambertian normalized reflectance and with a viewing geometry approximating the MISR instrument [9]. The image construction technique was similar to that described in the next section for the case using a variety of normalized directional reflectances. The aerosol in the atmospheric model had an opacity of 0.5, a single scattering albedo of unity and a phase function asymmetry parameter $g = 0.51$. The vertical distribution of the aerosol was exponential with a scale height of 2 km. The resulting Fourier transforms of the eight images, computed using a FFT-routine, are shown as amplitude (square root of power or absolute value) spectra of $\mathbf{I}$ in Fig. 1 for the lowest wavenumbers. Since direction dependent spatial structure is unimportant in the algorithm, a direction averaged wavenumber s was used, defined by $s = \left(u^2 + v^2\right)^{1/2}$. The amplitudes of those $\mathbf{I}$ with a common wavenumber s then were average together. The cosines of the nadir view angle are indicated, with the left-hand plot representing the MISR images from the forward-looking camera bank and the right-hand plot representing images from the aftward-looking bank. This figures illustrates both the non-Lambertian character and also the spatial uniformity of the surface directional reflectance.

Figs. 2(a–c) show the results of a sensitivity study of the retrieved functions $\mathbf{r}(0;\mu,\phi{-}\phi')$ and $|\mathbf{r}(s;\mu,\phi{-}\phi')|$ to the aerosol opacity. The curves in the figures are representations of the retrieved functions as defined by (4c) and (4d) and were computed at the view angles of the observations. The retrieved reflectances for both the forward and aftward viewing angle are plotted on the same $1/\mu$ half-axis for compactness. Goodness

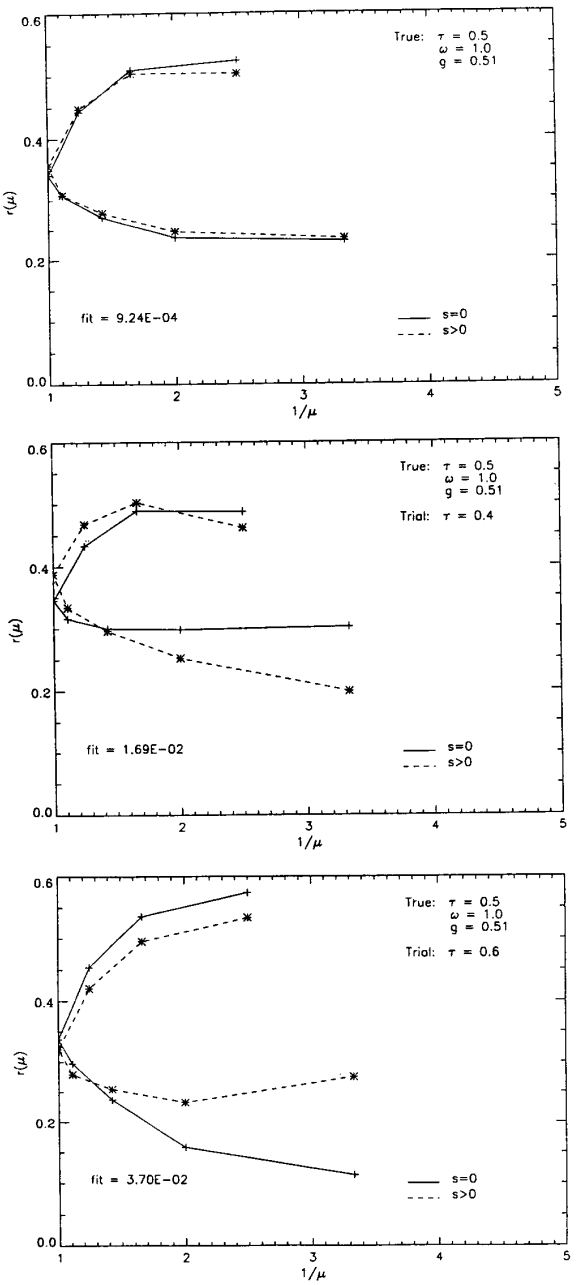

Fig. 2. Comparison of retrieved directional reflectance shapes using (a) the correct aerosol opacity of 0.5, (b) an incorrect opacity of 0.4, and (c) an incorrect opacity of 0.6.

of fit between zero and nonzero spatial frequency reflectance curves is described by the rms residuals (labeled "fit" in the figures) computed in the least squares analysis. Since the images have a spatially uniform angular variation, all wavenumbers $s > 0$ produce the same retrieved $|\mathbf{r}(s;\mu,\phi{-}\phi')|$ (aside from a scaling factor). Thus only one curve for $s > 0$ is illustrated in the figures.

Fig. 2(a) shows the retrieval results when all atmospheric

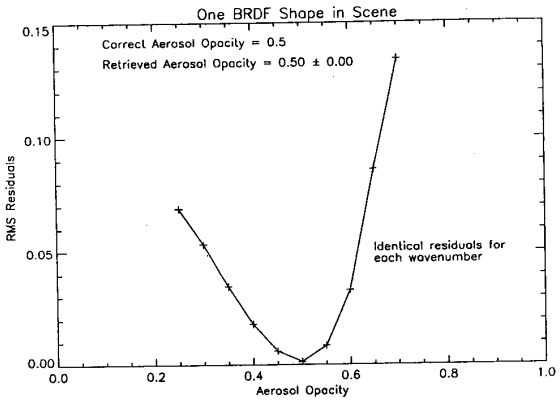

Fig. 3. Curve of retrieved directional reflectance shape comparison residuals. The best estimate of the aerosol opacity is at the minimum rms residual.

parameters are guessed correctly. The fact that the fit is not exact is due to the approximation used for the azimuth angle dependence of the directional reflectance as described by (3a) and (3b). The effects of errors in the guessed aerosol opacity are shown in Figs. 2(b) and 2(c). Only the opacity was incorrect; all other parameters in the atmospheric model remained fixed and were set to their true values. The figures clearly show that greater sensitivity to aerosol opacity is achieved when the larger view angles ($1/\mu > 2$) are available in the image data set. Fig. 3 summarizes the change in the rms residuals of the fit for a sequence of opacities ranging from 0.25 to 0.7. For this idealized image data set, it is clear that the aerosol opacity can be readily retrieved.

IV. Generalized Aerosol Retrieval Algorithm

For more realistic images with a surface described by a variety of different directional reflectances (i.e., r_n is also a function of the spatial coordinates), we can write

$$\mathbf{r}(0,0;\mu,\mu',\phi{-}\phi') = \mathbf{A}(u,v) \otimes \mathbf{r}_n(u,v;\mu,\mu',\phi{-}\phi') \quad \text{at } u,v=0 \quad (10a)$$

$$\mathbf{r}_n(u,v;\mu,\mu',\phi{-}\phi') = \mathbf{A}(u,v) \otimes \mathbf{r}_n(\mu,\mu',\phi{-}\phi') \quad (10b)$$

where (10a) and (10b) describe a convolution of the hemispherical albedo spectrum with the normalized directional reflectance spectrum. Now there is no obvious predictable relationship between the zero and nonzero wavenumber reflectances, even for the case where r_n and A are highly correlated. We make the assumption, however, that the aerosol retrieval algorithm for the single r_n case can be generalized to encompass the multi-r_n case. This generalization principle can be simply stated: Use the algorithm without change; treat the multi-r_n case as if only one r_n was present in the image set. The retrieved $|\mathbf{r}(s;\mu,\phi{-}\phi')|$ is actually described in (10) but will be handled as if was described by (4). The effect of this procedure is that the resulting rms residual curves for various wavenumbers will no longer be superimposed as in Fig. 3, but will tend to separate and take different shapes. The amount of

separation and shape variation will depend on the details of the convolution process in (10). The minimum variance condition will yield a different "best fit" atmosphere for each nonzero wavenumber used in the last squares analysis, but it is assumed that these different "best fit" atmospheres will tend to cluster about the true atmosphere. The ability of this generalized algorithm to perform effectively therefore implies that the $|\mathbf{r}(s;\mu,\phi-\phi')|$ retrieved for each wavenumber s becomes closer in angular shape to $\mathbf{r}(0;\mu,\phi-\phi')$ (the image-averaged normalized directional reflectance), in a statistical sense, when the guessed atmosphere approaches the true atmosphere.

To test soundness of the generalized aerosol retrieval algorithm, a simulated set of multi-angle images was generated using a calibrated Landsat Thematic Mapper image of the Wind River Basin area in Wyoming to specify, in a natural sense, the spatially variable hemispherical albedo. As a first step, a crude atmospheric correction was applied to the image. The darkest pixel in the scene was assumed to represent the path radiance and this value was then subtracted from all the pixels in the image. Although this does not provide a true atmospheric correction, we were merely interested in obtaining a realistic set of image values that could be interpreted as spatially varying surface hemispherical albedos. Next, the pixels were averaged, resulting in an image of 256 × 256 summed pixels. Thirty-eight different normalized directional reflectances, based on field measurements [10], were then applied to the individual pixels such that pixels with the same albedo were assigned the same directional reflectance function.

From this assignment of directional reflectances and albedos to the 256 × 256 pixels, a set of eight multi-angle simulated images was generated. The image view angles selected were those of the MISR instrument with the forward bank of cameras set at cosines of the view angle (μ) equal to 0.4, 0.6, 0.8, and 1.0 and the aftward camera bank set at 0.3, 0.5, 0.7, and 0.9. (Subsequent to performance of the calculations described in this paper, the number of cameras in the MISR instrument design was increased from eight to nine, with a nadir-viewing camera and four cameras each at symmetrical viewing angles in the fore and aft directions. In a practical sense, the results presented here will be unaffected by this change.) The azimuth angle of the aftward camera bank was defined to be 0°. This fixed the forward camera bank azimuth angle at 180°. The Sun in this coordinate system was positioned at a zenith angle of 38° and an azimuthal angle of 300°.

The effects of an atmosphere were then added to the multi-angle images according to (1). As a variation on the single r_n case described in the above section, the 1-D radiative transfer condition was assumed in the multi-r_n study. As noted in Section II, the upward diffuse transmittance T is then a delta function and the convolution operation produces the standard 1-D result of simple multiplication between the spatially invariant T and the directional reflectance r. All atmospheric fields, i.e., R, T, and I, were computed using a discrete ordinate code, with the atmosphere structured as a series of homogeneous layers. Aerosol characterization includes an exponential vertical distribution with a scale height of 2 km and a phase function which was moderately forward

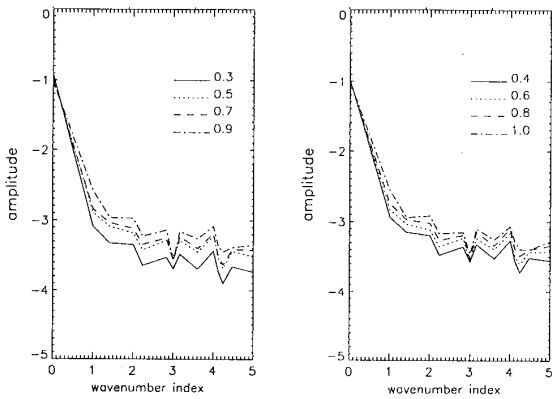

Fig. 4. Log of amplitude spectra for the simulated scene containing 38 directional reflectances.

scattering with an asymmetry parameter $g = 0.51$. The Rayleigh opacity component was 0.017 which corresponds to the 860-nm spectral channel of the MISR instrument. Two sets of images were made, one with an opacity of 0.2 and the other with an opacity of 0.5, each with an aerosol single scattering albedo equal to unity. A third set of images was also made for the case with an aerosol opacity of 0.5 and a single scattering albedo of 0.95.

The eight images of a given data set were then Fourier transformed using a FFT routine, resulting in a discrete $\mathbf{I}$ spectrum containing 128 wavenumbers in both the x- and y-directions. The amplitude spectrum of $\mathbf{I}$ vs. the directionally averaged wavenumber s for each of the eight images is shown in Fig. 4 for the case where the aerosol opacity equals 0.5 and the single scattering albedo equal unity. Like the single r_n case illustrated in Fig. 1, it can be seen that the amplitude (or power) spectra are strongly correlated because of the surface albedo pattern, but unlike Fig. 1 superimposed on that albedo pattern are the irregularities associated with the different directional reflectances encountered in the images.

Since the images were constructed using 1-D radiative transfer, (5a) and (5d) were used in the retrieval operation. Results of the generalized aerosol retrieval algorithm are shown in Fig. 5 for the image set with an opacity equal to 0.5. Each curve corresponds to a given wavenumber s ($s < 10$) and illustrates the sensitivity of the rms residuals, derived by shape comparison, to different guesses of the aerosol opacity. As in the single r_n case described in Section III, only the aerosol opacity was allowed to vary. All other parameters in the atmospheric model remained fixed and were set to the true values. Fig. 5 also illustrates the splitting apart or separation of the curves, due to the angular nonuniformity of the retrieved $|\mathbf{r}(s;\mu,\phi-\phi')|$. Nevertheless, these wavenumber-dependent directional reflectances apparently achieve their closest similarity to the retrieved zero wavenumber reflectance (minimum rms residual) when the guessed opacity is near the opacity of the true atmosphere, as suggested in the statement of the generalized retrieval algorithm. The opacity associated with the smallest residual of each curve is considered to be an estimate of the aerosol amount and so these opacity estimates

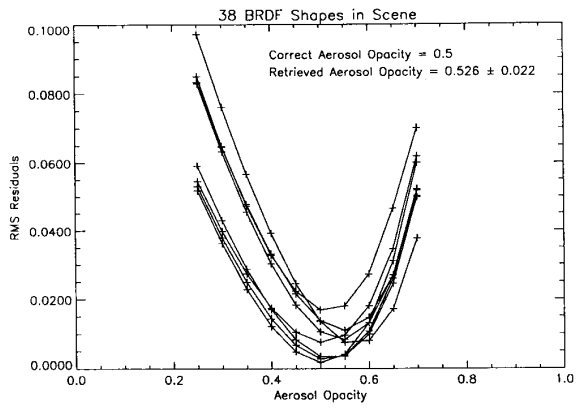

Fig. 5. Curves of retrieved directional reflectance shape comparison residuals for various spatial wavenumbers. The best estimate of the aerosol opacity is an average of the opacities at the minimum residual for each curve.

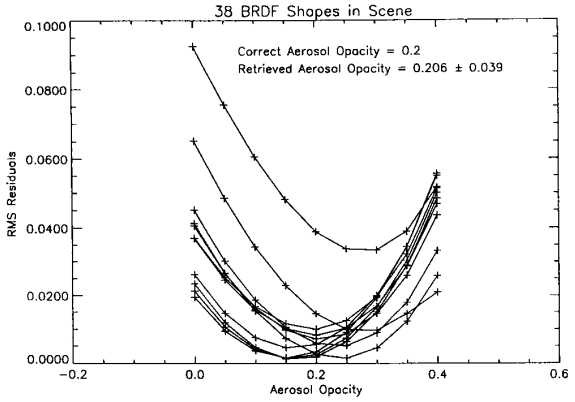

Fig. 6. Curves of retrieved directional reflectance shape comparison residuals for various spatial wavenumbers. The best estimate of the aerosol opacity is an average of the opacities at the minimum residual for each curve.

were averaged to obtain a value of 0.526 ± 0.022, in good agreement with the image atmospheric model.

Fig. 6 shows the rms residual curves of the image set with an aerosol opacity of 0.2. Compared to the previous aerosol opacity case, there is a wider spread in the estimated opacities from the individual curves, indicating less sensitivity to a smaller aerosol amount. The average opacity was determined to be 0.206 ± 0.039.

Finally, the sensitivity to aerosol single-scattering albedo is shown in Fig. 7 for the image set with a single scattering albedo of 0.95 and an opacity of 0.5. As in the two previous aerosol opacity cases, only the parameter of interest was varied. The average single-scattering albedo was determined to be 0.965 ± 0.0017. It generally has been very difficult to get good estimates of the aerosol single scattering albedo using satellite image data. The critical surface reflectance method of Fraser and Kaufman [11] uses nadir angle imagery of a scene observed under both clear and hazy conditions. The simultaneous, multi-angle imagery technique described here provides a complementary alternative.

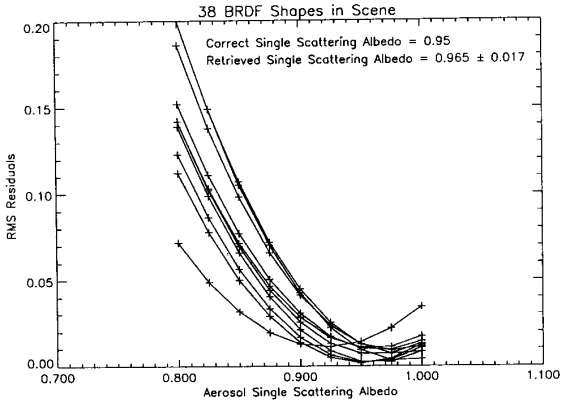

Fig. 7. Curves of retrieved directional reflectance shape comparison residuals for various spatial wavenumbers. The best estimate of the aerosol single scattering albedo is an average of the albedos at the minimum residual for each curve.

V. Discussion

Radiometrically calibrated multi-angle image data offer to the remote sensing community an additional dimension of information not obtainable with standard nadir or single angle image data. Using simulated multi-angle imagery, we have begun to assess the ability to atmospheric radiative transfer modeling to retrieve certain aerosol parameters, namely opacity and single scattering albedo. Although blurring (or adjacency) effects can be important in the analysis of images at high spatial resolution, we have considered here the less complex situation where 1-D radiative transfer theory is adequate. In any event, we assume that the atmosphere is horizontally homogeneous over a region of the image and that the surface albedo variations in that region then can be used to retrieve the aerosol properties. The amount of image contrast and how that contrast varies with view angle are the concepts we have exploited in an attempt to retrieve those atmospheric parameters which affect the surface radiance. We have used the Fourier transform as the operation which quantitatively assesses these image contrasts over the two-dimensional area of interest. Analysis of the resulting amplitude or power spectra, through the use of mathematical modeling of radiation transfer, then allows some measure of success in retrieving the desired atmospheric properties.

Once the atmospheric properties are retrieved over a region in a multi-angle image set, then the next task is to retrieve the surface directional reflectance for each pixel of the image in the region of interest. This process is straightforward for imagery in the 1-D radiative transfer regime. The directional reflectance for each pixel is considered to be a product of the hemispherical albedo $A(x, y)$ and a normalized directional reflectance $r_n(x, y; \mu, \phi - \phi')$ described by (3a). The functions $r^0(x, y; \mu)$ and $r^1(x, y; \mu)$ can be directly retrieved on a pixel-by-pixel basis by means of (5a) (where wavenumbers are replaced by spatial coordinates, except for T) and using the best estimate for the atmosphere. When the image is in the 3-D radiative transfer regime, then the directional reflectance retrieval is best carried out in Fourier domain for

each wavenumber coordinate u, v by means of (5a) and (5b) where $\mathbf{A}(u,v)r_n^0(\mu)$ and $\mathbf{A}(u,v)r_n^1(\mu)$ are replaced by the retrieved complex functions $\mathbf{r}^0(u,v;\mu)$ and $\mathbf{r}^1(u,v;\mu)$. After construction of $\mathbf{r}(u,v;\mu,\phi-\phi')$ using (3b), the result is inverse Fourier transformed back into the spatial domain. For both the 1-D and 3-D regimes, the directional reflectance r is best determined only at the observation angles of the image data. Use of (3a) to describe r at other angles is appropriate in the context of facilitating an angular integration but it could result in serious errors when it is interpreted as a reasonable stand-alone expression of the directional reflectance. It would be best at this point to employ a physical model for the directional reflectance, using the retrieved $r(x,y;\mu,\phi-\phi')$ at the observation angles as constraints on the model. A number of such physical models have recently appeared in the literature [12]–[14].

VI. Conclusion

The aerosol test cases described in this paper represent a very limited subset of the many possible atmospheric situations that can occur in remote sensing. We have shown, however, that multi-angle imaging data contains quantitative information about aerosols which can be retrieved, given certain constraints. These constraints took the form of knowledge about all the other parameters defining the aerosol condition in the atmosphere, except for the aerosol parameter being retrieved. In many locations around the world the aerosol meteorology is fairly well known [15], so that solving only for the aerosol amount, for example, would not be unreasonable. However, there is a far greater number of areas where little or nothing is known about the aerosol condition. To have some capability in being able to remotely sense these areas, we are currently investigating the potential of performing a simultaneous retrieval of a limited suite of aerosol parameters (e.g., opacity, single scattering albedo and one or two parameters pertaining to particle size distribution). The retrieval algorithm will be expanded to incorporate information obtained from the wavelength coverage of the MISR instrument. These efforts are expected to culminate in a series of retrieval algorithms that will be used for the routine processing of multi-angle image data to be returned by MISR after the launch of the Earth Observing System.

Acknowledgment

The authors thank Eric Danielson for computing assistance.

References

[1] D. J. Diner, C. J. Bruegge, J. V. Martonchik, T. P. Ackerman, R. Davies, S. A. W. Gerstl, H. R. Gordon, P. J. Sellers, J. Clark, J. A. Daniels, E. D. Danielson, V. G. Duval, K. P. Klaasen, G. W. Lilienthal, D. I. Nakamoto, R. J. Pagano, and T. H. Reilly, "MISR: A Multiangle Imaging SpectroRadiometer for geophysical and climatological research from Eos," *IEEE Trans. Geosci. Remote Sensing,* vol. GE-27, pp. 200–214, Mar. 1979.

[2] R. E. Dickinson, "Land surface processes and climate-surface albedos and energy balance," *Adv. Geophys.*, vol. 25, pp. 305–353, 1981.

[3] D. S. Kimes, P. J. Sellers, and D. J. Diner, "Extraction of spectral hemispherical reflectance (albedo) of surfaces from nadir and directional reflectance data," *Int. J. Rem. Sens.*, vol. 8, pp. 1727–1746, May 1987.

[4] H. R. Gordon, D. K. Clark, J. W. Brown, O. B. Brown, R. H. Evans, and W. W. Broenkow, "Phytoplankton pigment concentrations in the Middle Atlantic Bright: Comparison of ship determinations and CZCS estimates," *Appl. Opt.*, vol. 22, pp. 20–36, Jan. 1983.

[5] D. J. Diner and J. V. Martonchik, "Influence of aerosol scattering on atmospheric blurring of surface features," *IEEE Trans. Geosci. Remote Sensing,* vol. GE-23, pp. 618–624, Sept. 1985.

[6] D. J. Diner and J. V. Martonchik, "Atmospheric transfer of radiation above an inhomogeneous non-lambertian reflective ground. I. Theory," *J. Quant. Spectrosc. Radiat. Transfer,* vol. 31, pp. 97–125, Feb. 1984.

[7] D. J. Diner and J. V. Martonchik, "Atmospheric transfer of radiation above an inhomogeneous non-Lambertian reflecting ground-II. Computational considerations and results," *J. Quant. Spectros. Radiat. Transfer,* vol. 32, pp. 279–304, Oct. 1984.

[8] Y. J. Kaufman, "Atmospheric effect on spatial resolution of surface imagery: errata," *Appl. Opt.*, vol. 23, pp. 4164–4172, Nov. 1984.

[9] J. V. Martonchik, D. J. Diner, E. D. Danielson, and C. J. Bruegge, "Application of heterogeneous scene models to retrieval of land surface and atmospheric optical properties from space," in *Proc. IGARSS '90 Symposium.* New York: IEEE, pp. 179–182.

[10] D. S. Kimes, "Dynamics of directional reflectance factor distributions for vegetation canopies," *Appl. Opt.*, vol. 22, pp. 1364–1372, 1983.

[11] R. S. Fraser and Y. J. Kaufman, "The relative importance of scattering and absorption in remote sensing," *IEEE Trans. Geosci. Remote Sensing,* vol. GE-23, pp. 625–633, Sept., 1985.

[12] B. Pinty, M. M. Verstraete, and R. E. Dickinson, "A physical model for predicting bidirectional reflectances over bare soil," *Remote Sens. Environ.*, vol. 27, pp. 273–288, 1989.

[13] M. M. Verstraete, B. Pinty, and R. E. Dickinson, "A physical model for the bidirectional reflectance of vegetation canopies 1. Theory," *J. Geophys. Res.*, vol. 95, pp. 11755–11765, July, 1990.

[14] R. E. Dickinson, B. Pinty, and M. M. Verstraete, "Relating surface albedos in GCM to remotely sensed data," *Agricultural and Forest Meteorology,* vol. 52, pp. 109–131, 1990.

[15] G. A. d'Almeida, P. Koepke, and E. P. Shettle, *Atmospheric Aerosols: Global Climatology and Radiative Characteristics.* Hampton, VA: A. Deepak Publishing, 1991.

John V. Martonchik received the B.S. degree in physics from the Case Institute of Technology in 1964 and the Ph.D. degree in astronomy from the University of Texas at Austin in 1974.

He joined JPL in 1972 and is currently a member of the Technical Staff in the Atmospheric and Oceanographic Sciences Section. His experiences include telescopic and spacecraft observations of planetary atmospheres, laboratory and theoretical studies of the optical properties of gaseous, liquid, and solid materials, and development and implementation of one- and three-dimensional radiative transfer and line-by-line spectroscopy algorithms for studies of planetary atmospheres and Earth tropospheric remote sensing. He is currently an investigator in the NASA Remote Sensing Science Program and a coinvestigator on the EOS Multi-angle Imaging SpectroRadiometer experiment and the EOS Tropospheric Emission Spectrometer experiment.

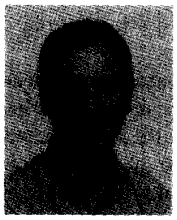

David J. Diner received the B.S. degree in physics with honors from the State University of New York at Stony Brook in 1973 and the M.S. and Ph.D. degrees in planetary science from the California Institute of Technology in 1977 and 1978, respectively.

He is currently a Technical Group Supervisor within the Atmospheric and Cometary Sciences Section at JPL. He has been involved in numerous NASA planetary and Earth remote-sensing investigations, as Principal- and Co-Investigator. He is currently a Principal Investigator within the NASA Remote Sensing Science Program, studying atmospheric effects on Earth remote sensing, and is also Principal Investigator of the EOS Multi-angle Imaging SpectroRadiometer experiment. Other research activities include investigation of imaging techniques for the detection of extrasolar planetary systems.

Dr. Diner is a member of the American Astronomical Society Division for Planetary Sciences.